ATLAS NOTE

ATLAS-CONF-2012-041

March 16, 2012

Further search for supersymmetry at $\sqrt{s} = 7$ TeV in final states with jets, missing transverse momentum and one isolated lepton

The ATLAS Collaboration

Abstract

This note presents an update and extension of the search for supersymmetry (SUSY) by the ATLAS experiment at the LHC in proton-proton collisions at a center-of-mass energy $\sqrt{s} = 7$ TeV in final states with jets, missing transverse momentum and one isolated electron or muon. The search is based on all data collected in 2011, with an integrated luminosity of 4.7 fb^{-1}. A new signal region is introduced to be sensitive to decay cascades of SUSY particles with small mass differences. A significant increase in sensitivity is obtained by simultaneously fitting mutually exclusive signal regions, and the shapes of distributions within those regions. Background uncertainties are constrained by fitting to the jet multiplicity distribution in background control regions. Observations remain consistent with Standard Model expectations, and limits are extended on a number of SUSY models.

1 Introduction

Supersymmetry (SUSY) [1–9] is a candidate for physics beyond the Standard Model (SM). If strongly interacting supersymmetric particles are present at the TeV-scale, they should be copiously produced in the 7 TeV collisions at the Large Hadron Collider [10]. In the minimal supersymmetric extension of the Standard Model [11–15] such particles decay into jets, leptons and the lightest supersymmetric particle (LSP) which can be weakly interacting and escape detection, leading to missing transverse momentum ($\vec{p}_T$ and its magnitude E_T^{miss}) in the final state. Significant E_T^{miss} can also arise in scenarios where the LSP decays to final states containing neutrinos, or in scenarios where neutrinos are created somewhere in the SUSY decay cascade.

This note presents an update of the search with the ATLAS detector for SUSY in final states containing jets, one isolated lepton (electron or muon) and E_T^{miss}. Previous searches in this channel have been conducted by both the ATLAS [16] and CMS [17] collaborations with an integrated luminosity of 1 fb^{-1}. In this note, the analysis is extended to 4.7 fb^{-1}. Other improvements with respect to the previous ATLAS analysis include a new signal region with a soft lepton and soft jets in order to probe SUSY decay spectra involving small mass differences, and for the first time in ATLAS SUSY searches, the use of a simultaneous fit to multiple signal regions and to the shapes of distributions within those signal regions. Background uncertainties are constrained by fitting to the jet multiplicity distribution in background control regions.

2 The ATLAS Detector

The ATLAS detector [18, 19] consists of a tracking system (inner detector, or ID) surrounded by a thin superconducting solenoid providing a 2T magnetic field, electromagnetic and hadronic calorimeters and a muon spectrometer (MS). The ID consists of pixel and silicon microstrip detectors, surrounded by the transition radiation tracker (TRT). The electromagnetic calorimeter is a lead liquid-argon (LAr) detector. Hadron calorimetry is based on two different detector technologies, with scintillator-tiles or LAr as active media, and with either steel, copper, or tungsten as the absorber material. The MS is based on three large superconducting toroids arranged with an eight-fold azimuthal coil symmetry around the calorimeters, and a system of three stations of chambers for the trigger and for precise measurements. The nominal pp interaction point at the center of the detector is defined as the origin of a right-handed coordinate system. The positive x-axis is defined by the direction from the interaction point to the center of the LHC ring, with the positive y-axis pointing upwards, while the beam direction defines the z-axis. The azimuthal angle ϕ is measured around the beam axis and the polar angle θ is the angle from the z-axis. The pseudorapidity is defined as $\eta = -\ln\tan(\theta/2)$.

3 SUSY Signal Modeling and Simulated Event Samples

Simulated event samples are used for estimating the signal acceptance, the detector efficiency, and for estimating many of the backgrounds. As in Ref. [16], the SUSY models considered are MSUGRA/CMSSM [20, 21] with $\tan\beta = 10$, $A_0 = 0$ and $\mu > 0$, and simplified models [22, 23]. This analysis is focused on the simplified model with a particle content consisting of the gluino, and the lightest chargino and neutralino, where the gluino decays to the neutralino LSP via the intermediate step ("one-step") of the lightest chargino. The chargino decays by real or virtual W emission where the W decays according to SM branching ratios. The chargino mass is set to be halfway between the gluino and LSP masses. Further details of these models are described in Ref. [16]. The MSUGRA/CMSSM signal samples are generated with HERWIG++ 2.5.2 [24]; ISAJET 7.80 [25] is used to generate the physical particle masses. The simplified models are generated with one extra jet in the matrix element using MADGRAPH5 [26], interfaced to PYTHIA, and parton density functions (PDFs) from CTEQ6L1 [27]; MLM matching [28] is done with a scale parameter that is the smaller of either 50 GeV or the mass of the lightest sparticle in the hard-scattering matrix element. Signal cross sections are calculated to next-to-leading order in the strong coupling constant, including the resummation of soft gluon emission at next-to-leading-logarithmic accuracy (NLO+NLL) [29–33].[1]

Physics process	Generator	Cross section (nb)	Calculation	
$t\bar{t}$	ALPGEN 2.13 [34]	0.165	NLO+NLL	[35]
$W(\rightarrow \ell\nu)$ + jets	ALPGEN 2.13 [34]	10.46	NNLO	[36]
$Z/\gamma^{*}(\rightarrow \ell\ell)$ + jets ($m_{\ell\ell} > 40$ GeV)	ALPGEN 2.13 [34]	1.07	NNLO	[36]
$Z/\gamma^{*}(\rightarrow \ell\ell)$ + jets (10 GeV < $m_{\ell\ell}$ < 40 GeV)	ALPGEN 2.13 [34]	3.97	NNLO	[36]
Single-top (t-chan)	MC@NLO 4.01 [37]	0.0071	NLO	
Single-top (s-chan)	MC@NLO 4.01 [37]	0.0005	NLO	
Single-top (Wt-chan)	MC@NLO 4.01 [37]	0.0146	NLO	
WW	HERWIG 6.5.20 [38]	0.0449	NLO	[39]
WZ ($66 < M_Z < 116$ GeV)	HERWIG 6.5.20 [38]	0.0180	NLO	[39]
ZZ ($M_Z > 60$ GeV)	HERWIG 6.5.20 [38]	0.0060	NLO	[39]

Table 1: Simulated background event samples used in this analysis, and the production cross sections. The ALPGEN samples are generated with $0 \leq N_{\mathrm{parton}} \leq 5$ in the matrix element. The W+jets and Z/γ^{*}+jets samples are normalized using the inclusive cross sections multiplied by the relevant branching ratio; the values shown in the table are for a single lepton flavor. The single-top cross sections are taken from MC@NLO; for the s- and t-channels, they are listed for a single lepton flavor. Details of PDF sets and underlying event tunes are given in the text.

The simulated event samples for the SM backgrounds are summarized in Table 1. The $t\bar{t}$, W+jets and Z+jets samples are normalized using the inclusive cross sections. The ALPGEN samples are generated with the MLM matching scheme. Parton shower and fragmentation processes are simulated for the ALPGEN and MC@NLO samples using HERWIG [38] with JIMMY [40] for underlying event simulation. The PDFs used in this analysis are: CTEQ6L1 [27] for the ALPGEN samples, CT10 [41] for MC@NLO, and MRSTMCal (LO^{**}) [42] for HERWIG. The underlying event tunes are the ATLAS AUET2 tunes [43]. The theoretical cross sections for W+jets and Z+jets are calculated with FEWZ [36] with the MSTW2008NNLO [44] PDF set. For the diboson cross sections, MCFM [39] with the MSTW2008NLO PDFs is used. The $t\bar{t}$ cross section is calculated with HATHOR 1.2 [35] using MSTW2008NNLO PDFs.

The detector simulation [45] is performed using GEANT4 [46]. All simulated samples are generated with a range of simulated minimum-bias interactions overlaid on the hard-scattering event to account for the multiple pp interactions in the same beam crossing (pile-up). The overlay also treats the impact of pile-up on beam crossings other than the one in which the event occurred. Scale factors are applied to the simulated samples to adjust for differences between data and simulation for the lepton trigger and

[1] The NLL correction is used for squark and gluino production when the squark and gluino masses lie between 200 GeV and 2 TeV. Following the convention used in the NLO calculators the squark mass is defined as the average of the squark masses in the first two generations. In the case of gluino-pair (associated squark-gluino) production processes, the NLL calculations are extended up to squark masses of 4.5 TeV (3.5 TeV). For masses outside this range and for other types of production processes (i.e. electroweak and associated strong and electroweak) cross sections at NLO accuracy obtained with PROSPINO (v2.1) [29] are used.

reconstruction efficiencies, and for the efficiency and mis-tag rates for b-tagging.

For the ALPGEN W+jets sample, the transverse momentum (p_{T}) of the vector boson is reweighted at the generator level. The weights are derived from a comparison at the generator level of the p_{T} of the W-boson between ALPGEN and SHERPA (v1.3.1) [47] where the latter are generated with the same CTEQ6L1 PDF set as the fully-simulated ALPGEN samples. This reweighting procedure is found to improve the agreement between data and simulation in control regions populated by W+jets events, and overcomes the limited statistics in the SHERPA simulated samples. The weights are cross-checked by comparing the kinematic distributions between data and simulation in Z+jets events and in statistically independent W+jets control samples.

4 Object Reconstruction

This analysis is based on two broad classes of event selection: *i)* 3-jet and 4-jet analyses that are an extension to higher masses of the previous search [16], and *ii)* a soft-lepton analysis geared towards SUSY models with small mass differences in the decay cascade. The event selection requirements will be described in detail in Section 6. Here we describe the final-state object reconstruction and selection requirements.

4.1 Lepton selection in 3- and 4-jet analyses

Electrons are reconstructed from clusters in the electromagnetic calorimeter matched to a track in the ID [48]. For the final selection of signal events, "signal" electrons are required to pass a variant of the "tight" selection of [48], providing 1-2% gain in efficiency and slightly better background rejection. Signal electrons must have $p_{\mathrm{T}} > 25$ GeV, $|\eta| < 2.47$ and a distance to the closest jet $\Delta R = \sqrt{(\Delta\eta)^2 + (\Delta\phi)^2}$ to be $\Delta R < 0.2$ or $\Delta R > 0.4$; the jets considered at this stage are not required to be associated with the event primary vertex. Electrons with $\Delta R < 0.2$ are kept, and the jet is discarded. The jets used in this ΔR requirement have p_{T} >20 GeV and $|\eta| < 4.5$. Signal electrons are required to pass further criteria on the electron isolation: the scalar sum of the p_{T} of tracks within a cone of radius $\Delta R = 0.2$ around the electron (excluding the electron itself) is required to be less than 10% of the electron p_{T}.

Muons are identified either as a combined track in the MS and ID systems, or as an ID track matching with a MS segment [49,50]. Requirements on the quality of the ID track are identical to those in Ref. [16]. Muons in the final selection ("signal" muons) are required to have $p_{\mathrm{T}} > 20$ GeV, $|\eta| < 2.4$ and $\Delta R > 0.4$ with respect to the closest jet where the requirements on the jets are the same as in the electron case. Further isolation criteria are imposed: the scalar sum of the p_{T} of tracks within a cone of radius $\Delta R = 0.2$ around the muon candidate (excluding the muon itself) is required to be less than 1.8 GeV.

4.2 Soft-lepton selection

Signal electrons for the soft-lepton analysis are defined as above except that they are required to have p_{T} between 7 and 25 GeV and be outside the transition region between the barrel and endcap calorimeter ($1.37 < |\eta| < 1.52$). Signal muons for the soft-lepton analysis are defined as above except that they must have p_{T} between 6 and 20 GeV.

4.3 Common definitions

Jets are reconstructed using the anti-k_t algorithm [51, 52] with a radius parameter $R = 0.4$. Jets arising from detector noise, cosmic rays or other non-collision sources are rejected [53]. To take into account the differences in calorimeter response between electrons and hadrons, a p_{T}- and η-dependent factor, derived from simulated events, is applied to each jet to provide an average energy scale correction [53] back to particle-level.

Signal jets are required to have $p_T > 25$ GeV and $|\eta| < 2.5$. In addition, signal jets are required to be associated with the hard-scattering of interest, by demanding that at least 75% of the scalar sum of the p_T of all tracks associated with the jet must come from tracks associated to the primary vertex of the event; unlike the previous analysis, jets with no associated tracks are rejected in order to cope with the higher pile-up conditions. Approximately 10% of the jets are removed by these tracking requirements. The primary vertex [54] is required to be consistent with the beamspot envelope and to have at least five tracks; when more than one such vertex is found, the vertex with the largest summed $|p_T|^2$ of the associated tracks is chosen.

The missing transverse momentum is computed as the opposite of the vector sum of the p_T of all jets with $p_T >$20 GeV and $|\eta| < 4.5$, the signal lepton (p_T requirement lowered to 20 GeV and identification requirements loosened to "medium" for electrons), any additional non-isolated muons with $p_T > 10$ GeV and $\Delta R > 0.3$ with respect to the closest jet, and any calorimeter clusters with $|\eta| < 4.9$ that are not associated to any of the above-mentioned objects. The non-associated clusters are evaluated at the electromagnetic energy scale.

For approximately 20% of the 2011 data-taking run, an electronics failure created a region in the barrel electromagnetic calorimeter where no signals could be read out, corresponding to an area of 1.4×0.2 in $\eta \times \phi$ space. Events with an electron in this region are vetoed for the entire dataset, leading to an acceptance loss of less than 1% for signal events in the signal region. For jets, the amount of transverse energy (E_T) lost in the dead region can be estimated from the energy depositions in the neighboring calorimeter cells. If this lost E_T projected along the E_T^{miss} direction amounts to more than 10 GeV and constitutes more than 10% of the E_T^{miss} the event is rejected. The effect of the electronics failure is fully described in the detector simulation, and the loss of signal acceptance from this requirement is found to be negligible.

Jets arising from b-quarks are identified using information about track impact parameters and reconstructed secondary vertices [55]; the b-tagging algorithm is based on a neural network using the output weights of the JetFitter+IP3D, IP3D, and SV1 (defined in Ref. [55]) algorithms as input. The b-tagging requirements are set at an operating point with an average efficiency of 60% for b-jets in simulated $t\bar{t}$ events, for which the algorithm provides a rejection factor of approximately 200-400 for light-quark and gluon jets and a rejection of approximately 7-10 for charm jets.

5 Trigger and Data Collection

The data used in this analysis were collected from March through October 2011 during which the instantaneous luminosity of the LHC reached as high as $3.65 \times 10^{33}\text{cm}^{-2}\text{s}^{-1}$. The average number of expected interactions per beam crossing ranged from approximately 4 to 16, with an average of 10. After the application of beam, detector, and data-quality requirements, the total integrated luminosity is 4.7 fb^{-1}. The uncertainty on the luminosity determination is estimated to be 3.9% [56, 57].

Three types of triggers were used to collect the data: electron, muon and E_T^{miss}. The electron trigger selects events containing one or more electron candidates, based on the presence of a cluster in the electromagnetic calorimeter, with a shower shape consistent with that of an electron. The transverse energy threshold at the trigger level ranged between 20-22 GeV, depending on the luminosity. For signal electrons satisfying $p_T > 25$ GeV, the trigger efficiency is in the plateau region and ranges between 95% and 97%. In order to recover some of the efficiency for high-p_T electrons during running periods with the highest luminosity, events were also collected with an electron trigger with looser shower shape requirements but with a p_T threshold of 45 GeV.

The muon trigger selects events containing one or more muon candidates based on tracks identified in the MS and ID. The muon trigger p_T threshold was 18 GeV. During running periods with the highest luminosity, the lowest level muon trigger was tightened by requiring a three-MS-station coincidence rather than two; in order to recover some of the resulting inefficiency, events were also collected with a muon trigger which maintained the two-station coincidence but required in addition a jet with an p_T greater than 10 GeV evaluated at the electromagnetic scale.[2] This jet requirement is fully efficient for offline jets with p_T greater than approximately 50 GeV. The muon triggers reach plateau below the signal muon p_T threshold of 20 GeV. The plateau efficiency ranges from about 70% in the barrel region to 88% in the endcaps.

The E_T^{miss} trigger required an E_T^{miss}> 60 GeV at the electromagnetic scale. This trigger reaches the efficiency plateau for offline calibrated E_T^{miss} > 180 GeV. The efficiency at the plateau is close to 100%.

6 Event Selection

Two variables, derived from the kinematic properties of the reconstructed objects, are used in the event selection. The transverse mass (m_T) of the lepton (ℓ) and $\vec{p}\!\!\!/_T$ is defined as

$$m_T = \sqrt{2p_T^{\ell} E_T^{miss}(1 - \cos(\Delta\phi(\vec{\ell}, \vec{p}\!\!\!/_T)))}$$

The inclusive effective mass (m_{eff}^{inc}) is the scalar sum of the p_T of the lepton, the jets and E_T^{miss}:

$$m_{eff}^{inc} = p_T^{\ell} + \sum_{i=1}^{N_{jet}} p_{T,i} + E_T^{miss}$$

where the index i runs over all the signal jets in the event. It is also useful to define $H_T = m_{eff}^{inc} - E_T^{miss}$. Note that unlike the analysis in Ref. [16] the sum runs over all signal jets, rather than just the three or four leading-p_T jets, in order to improve the signal discrimination. The inclusive effective mass is correlated with the overall mass scale of the hard-scattering and provides good discrimination against SM background, without being too sensitive to the details of the SUSY decay cascade. A sum over the 2-, 3-, or 4-leading p_T jets, depending on the minimum number of jets required in the signal region, is used to compute m_{eff} and the ratio E_T^{miss}/m_{eff}. The latter is similar to the E_T^{miss} significance in that it reflects the change in the E_T^{miss} resolution as a function of the calorimeter activity in the event; the definition selected here improves the rejection of background from mismeasured jets.

This analysis is based on three signal regions, each tailored to maximize the sensitivity to different SUSY event topologies:

1. *3-jet selection.* Events are collected with the electron and muon triggers. The number of signal leptons (electron or muon) is required to be exactly one. Events containing additional leptons are rejected in this analysis. For this purpose the "medium" electron selection as defined in Ref. [48] is used, the p_T requirement is lowered to 10 GeV and the track isolation is not applied; for muons, the p_T threshold is lowered to 10 GeV and the track isolation requirement is removed. The number of jets is required to be ≥ 3, with a leading jet satisfying p_T > 100 GeV and the other jets having p_T > 25 GeV. Events with four or more jets are rejected if the fourth jet of the p_T-ordered jets has p_T > 80 GeV; this requirement keeps this signal region disjoint from the 4-jet signal region. In addition, the following are required: m_T > 100 GeV, E_T^{miss} > 250 GeV, E_T^{miss}/m_{eff} > 0.3, and m_{eff}^{inc} > 1200 GeV.

[2]The electromagnetic scale is the basic calorimeter signal scale for the ATLAS calorimeters. It has been established using test-beam measurements for electrons and muons to give the correct response for the energy deposited in electromagnetic showers, while it does not correct for the lower response of the calorimeter to hadrons.

	3-jet	**4-jet**	**soft-lepton**
Trigger	Single electron or muon (+jet)		Missing E_{T}
N_{lep}	1	1	1
p_{T}^{ℓ} (GeV)	> 25 (20)	> 25 (20)	[7,25] ([6,20])
$p_{\mathrm{T}}^{\ell_2}$(GeV)	< 10	< 10	< 7 (6)
N_{jet}	≥ 3	≥ 4	≥ 2
p_{T}^{jet} (GeV)	> 100, 25, 25	> 80, 80, 80, 80	> 130,25
$p_{\mathrm{T}}^{jet\ 4}$ (GeV)	< 80	—	—
$E_{\mathrm{T}}^{\mathrm{miss}}$ (GeV)	> 250	> 250	> 250
m_{T} (GeV)	> 100	> 100	> 100
$E_{\mathrm{T}}^{\mathrm{miss}}/m_{\mathrm{eff}}$	> 0.3	> 0.2	> 0.3
$m_{\mathrm{eff}}^{\mathrm{inc}}$ (GeV)	> 1200	> 800	—

Table 2: Overview of the selection criteria for the signal regions in this analysis. The p_{T} selections for leptons are given for electrons (muons).

2. *4-jet selection*. Similar to the above, events are collected with the electron and muon triggers. The number of signal leptons (electron or muon) is required to be exactly one. Events containing additional leptons are rejected, using the same criteria as in the 3-jet channel. The number of jets is required to be ≥ 4, with the four leading jets satisfying $p_{\mathrm{T}} > 80$ GeV. In addition, the following requirements are applied: $m_{\mathrm{T}} > 100$ GeV, $E_{\mathrm{T}}^{\mathrm{miss}} > 250$ GeV, $E_{\mathrm{T}}^{\mathrm{miss}}/m_{\mathrm{eff}} > 0.2$, and $m_{\mathrm{eff}}^{\mathrm{inc}} > 800$ GeV.

3. *soft-lepton selection*. Events are collected with the $E_{\mathrm{T}}^{\mathrm{miss}}$ triggers. The number of signal leptons (electron or muon) is required to be exactly one. Electrons are required to have 7 GeV < p_{T} < 25 GeV, and muons are required to be in the range 6 GeV < p_{T} < 20 GeV. Events containing an additional electron (muon) with $p_{\mathrm{T}} > 7$ (6) GeV are rejected; as in the 3- and 4-jet analyses, no track isolation requirements are applied when selecting leptons for vetoing purposes. The number of jets is required to be ≥ 2, with the leading jet satisfying $p_{\mathrm{T}} > 130$ GeV and the second jet having $p_{\mathrm{T}} > 25$ GeV. In addition, the following are required: $m_{\mathrm{T}} > 100$ GeV, $E_{\mathrm{T}}^{\mathrm{miss}} > 250$ GeV, and $E_{\mathrm{T}}^{\mathrm{miss}}/m_{\mathrm{eff}} > 0.3$. No explicit requirement on $m_{\mathrm{eff}}^{\mathrm{inc}}$ is applied.

The 3- and 4-jet signal regions are extensions of the previous analysis [16] to higher SUSY mass scales. They have been optimized for the MSUGRA/CMSSM model as well as for the bulk of the one-step simplified models with large mass difference (ΔM) between the gluino and the LSP. The soft-lepton signal region targets the simplified models with small Δm; the hard leading jet for this signal region comes from initial-state radiation (ISR). Another significant difference compared to the analysis of [16] is that none of the current analysis channels impose a requirement on the azimuthal angle between the $E_{\mathrm{T}}^{\mathrm{miss}}$ vector and any of the jets. This adds sensitivity to SUSY decay chains where the LSP is boosted along the jet direction. The selection criteria are summarized in Table 2.

7 Background Estimation

The dominant sources of background in this analysis are: *i)* semi- and fully-leptonic $t\bar{t}$ (where in the latter, one lepton is lost or mis-identified), and *ii)* W+jets where the W decays leptonically. Other background processes which are considered are multijets, Z+jets, single-top and dibosons.

The major backgrounds ($t\bar{t}$ and W+jets) are estimated by isolating each process in a control region, normalizing the simulation to the event counts in the control region, and then using the simulation to extrapolate into the signal region. The multijet background is estimated entirely from the data by a matrix method described below, where one or more of the lepton identification criteria are inverted (with all other signal event selection criteria applied) and the resulting yield is multiplied by the probability for a jet to be mis-identified as an isolated lepton. All other (smaller) backgrounds are estimated entirely from the simulation, using the most accurate theoretical cross sections available.

A new feature of this analysis is the splitting of the control regions into jet multiplicity bins in order to constrain some of the shape uncertainties for W+jets and $t\bar{t}$ backgrounds when extrapolating from control to signal regions.

7.1 W+jets and $t\bar{t}$ Control Regions

The W+jets and $t\bar{t}$ processes are isolated in control regions defined by the following requirements. For both the 3- and 4-jet analyses, ≥ 3 jets are required, with a leading jet $p_{\mathrm{T}} > 80$ GeV and the other jets above 25 GeV. The lepton requirements are the same as in the signal region. However, the $E_{\mathrm{T}}^{\mathrm{miss}}$ is required to be between 30 and 120 GeV while the transverse mass is required to be between 40 and 80 GeV. Furthermore, the $m_{\mathrm{eff}}^{\mathrm{inc}}$ requirement is relaxed to be > 400 GeV. The W+jets and $t\bar{t}$ control regions are distinguished by requirements on the number of b-tagged jets. For the W+jets control region, events are rejected if any of the 3 highest p_{T} jets is b-tagged; the rejected events then define the $t\bar{t}$ control region. Table 3 summarizes the control regions definitions and Figure 1 top left (right) shows the composition of the W+jets ($t\bar{t}$) control regions. Numerical results on the composition of the control regions are presented in Tables 4 and 5 of Section 9.

	3- and 4-jet W control	**3- and 4-jet $t\bar{t}$ control**	**soft-lepton W control**	**soft-lepton $t\bar{t}$ control**
N_{jet}	≥ 3	≥ 3	Same as signal region	
p_{T}^{jet} (GeV)	> 80, 25, 25	> 80, 25, 25	Same as signal region	
N_{jet} (b-tagged)	0	≥ 1	0	≥ 1
$E_{\mathrm{T}}^{\mathrm{miss}}$ (GeV)	[30,120]	[30,120]	[180,250]	[180,250]
m_{T} (GeV)	[40,80]	[40,80]	[40,80]	[40,80]
$m_{\mathrm{eff}}^{\mathrm{inc}}$ (GeV)	> 400	> 400	—	—

Table 3: Overview of the selection criteria for the W+jets and $t\bar{t}$ control regions in this analysis. Only the criteria which are different from the signal selection criteria of Table 2 are shown.

For the soft-lepton analysis, the control region requirements on the leptons and jets are the same as in the signal region. However, the $E_{\mathrm{T}}^{\mathrm{miss}}$ is required to be between 180 and 250 GeV and the transverse mass is required to be between 40 and 80 GeV. Again, the W+jets and $t\bar{t}$ control regions are distinguished by the presence of b-tagged jets. For W+jets, events are rejected if any of the two highest p_{T} jets is b-tagged; the rejected events form the $t\bar{t}$ control region. Figure 2 shows the composition of the W+jets and $t\bar{t}$ control regions as a function of $E_{\mathrm{T}}^{\mathrm{miss}}$ in the soft-lepton channel.

7.2 Multijet Background

Multijet events become a background when a jet is misidentified as an isolated lepton or when a real lepton appears as a decay product of hadrons in jets but is sufficiently isolated, for example from $b-$ or $c-$ jets. Such lepton-like objects are collectively referred to as misidentified leptons in this note. The multijet background in the signal region, and in the W+jets and $t\bar{t}$ control regions where it is more

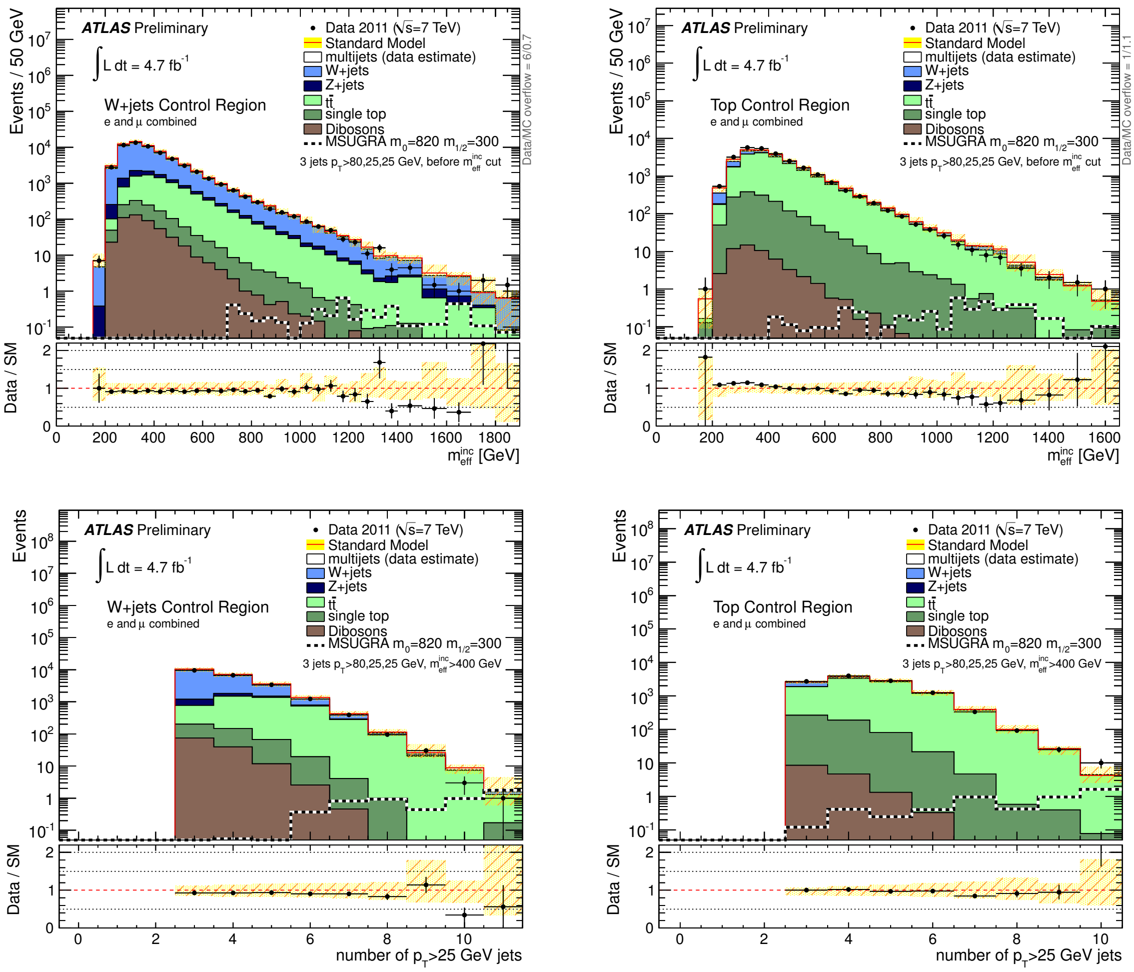

Figure 1: Top left (right): $m_{\text{eff}}^{\text{inc}}$ distribution in the W+jets ($t\bar{t}$) control region in data and simulation for the 3- and 4-jet analyses. Bottom left (right): Distribution of the number of jets in the W+jets ($t\bar{t}$) control region; the last bin is inclusive and includes all overflows. The electron and muon channels have been combined in all distributions shown here. The "Data/SM" plots show the ratio between data and the summed Standard Model expectation. The expectation for multijets is derived from the data. The remaining Standard Model expectation is derived from simulation only, normalized to the theoretical cross sections. The uncertainty band on the Standard Model expectation shown here combines the statistical uncertainty on the simulated event samples with the systematic uncertainties on the jet energy scale, b-tagging, data-driven multijet background, and luminosity. The systematic uncertainties are largely correlated from bin to bin.

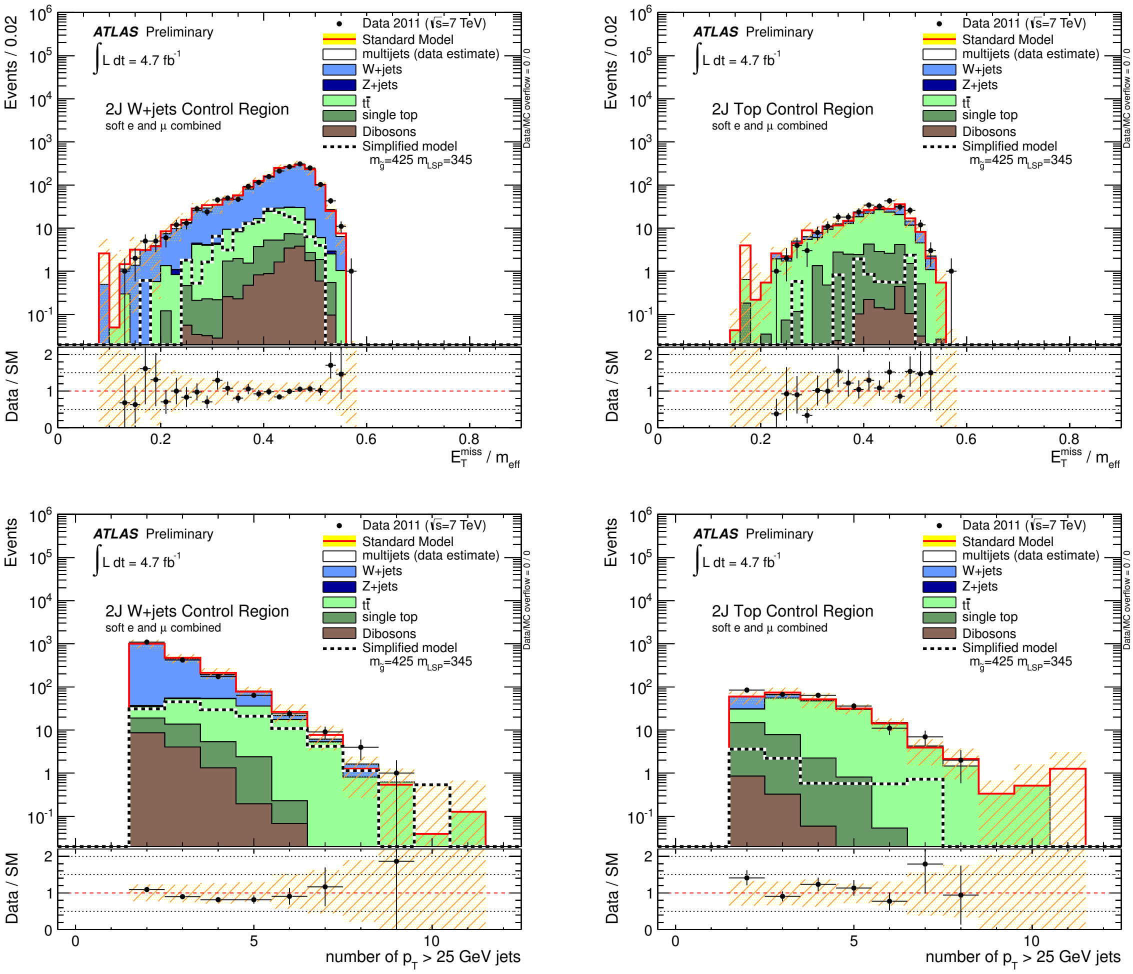

Figure 2: Top: $E_{\mathrm{T}}^{\mathrm{miss}}/m_{\mathrm{eff}}$ distribution in the W+jets (left) and $t\bar{t}$ (right) control regions in data and simulation for the soft-lepton analysis. Bottom: Jet multiplicity distribution in the W+jets (left) and $t\bar{t}$ (right) control regions. In all distributions, electron and muon channels have been combined. The “Data/SM” plots show the ratio between data and the summed Standard Model expectation. The expectation for multijets is derived from the data. The remaining Standard Model expectation is derived from simulation only, normalized to the theoretical cross sections. The uncertainty band on the Standard Model expectation shown here combines the statistical uncertainty on the simulated event samples with the systematic uncertainties on the jet energy scale, b-tagging, data-driven multijet background, and luminosity. The systematic uncertainties are largely correlated from bin to bin.

significant, is estimated from the data following a matrix method similar to that employed in Ref. [16]. Only the key ingredients of the measurement will be described here.

The multijet background from all sources (but separated by lepton flavor) is determined collectively. The multijet process is enhanced in a control sample with all the SUSY signal region criteria applied but where the lepton isolation criteria are not imposed and the shower shape requirements on electrons have been slightly relaxed. The lepton misidentification efficiency, defined as the fraction of events passing the lepton isolation criteria, is estimated as follows.

For electrons (muons) with $p_{\rm T} > 25$ (20) GeV the misidentification efficiency is estimated with events containing at least one electron (muon) satisfying the relaxed criteria, and at least one signal jet with $p_{\rm T} > 30$ (60) GeV. In addition for the electron case, $E_{\rm T}^{\rm miss} < 30$ GeV is required. For the muon case, the event is required to contain exactly one muon with $|d_0|/\sigma_{d_0} > 5$ where d_0 and σ_{d_0} are the transverse impact parameter and its uncertainty, respectively, measured with respect to the primary vertex. For the soft-lepton analysis, the sample for the misidentification efficiency determination is based on events containing a same-sign and same-flavor lepton pair where the leptons satisfy the relaxed isolation criteria. The same-sign requirement reduces the contamination from true leptons and enhances the background. One of the leptons is required to fail the signal lepton criteria to further enhance the background; the misidentification efficiency is measured with the other lepton. An additional veto around the Z-boson mass is applied.

7.3 Other Backgrounds

The background from Z+jets, single-top and diboson production is estimated almost purely from simulation. The background from cosmic ray muons overlapping a hard-scattering event is estimated from a control sample with large z_0, defined as the distance in the z direction with respect to the primary vertex, evaluated at the point of closest approach of the muon to the primary vertex in the transverse plane. Extrapolating to the signal region $|z_0| < 5$ mm, the contribution is found also to be negligible.

8 Systematic Uncertainties on the Background

Systematic uncertainties have an impact on the expected event yields in the control regions and on the extrapolation factors used to derive the background yields in the signal region. The following detector-related systematic uncertainties are taken into account. The jet energy scale (JES) uncertainty has been determined from a combination of test beam, simulation and in-situ measurements from 2010 pp collision data [53]. Additional contributions to the JES uncertainty arising from the higher luminosity and pile-up in 2011 are taken into account. Uncertainties on the lepton identification, momentum/energy scale and resolution are estimated from samples of $Z \to \ell^+\ell^-$, $J/\psi \to \ell^+\ell^-$ and $W^\pm \to \ell^\pm\nu$ decays. The uncertainties on the jet and lepton energies are propagated to the $E_{\rm T}^{\rm miss}$; an additional $E_{\rm T}^{\rm miss}$ uncertainty arising from energy deposits not associated to any reconstructed objects is also included [58]. Uncertainties on the b-tagging efficiency are derived from data samples tagged with muons associated to jets [55]. Uncertainties from the identification of jets associated with the primary vertex and from the overlay of pile-up in simulated events are both found to be negligible.

Theoretical modeling uncertainties in the simulation include the following. Renormalization and factorization scales (and in the case of ALPGEN, the scale for α_S in the matching process) are independently varied by a factor of two, up and down from their nominal settings. The renormalization and factorization scales mostly affect the overall normalization of the cross section; the effect is mainly removed by normalizing the simulation to the data in control regions. The effect of the matching scale variations (parametrized by $k_{T_{fac}}$) is to change the relative normalization of each of the ALPGEN $N_{\rm parton}$ samples. An additional parameter for the MLM matching, the jet $p_{\rm T}$ threshold used in the matching

($p_{\mathrm{T,min}}$), is shifted from its default value of 15 GeV to 30 GeV. The uncertainty due to the reweighting of the p_{T} of the W in the ALPGEN samples is estimated by removing the reweighting.

9 Background Fit

The background in the signal region is estimated with a fit based on the profile likelihood method [59]. The inputs to the fit are as follows:

1. The observed number of events in the W and $t\bar{t}$ control regions, and the number expected from simulation, separated into 7 (8) jet multiplicity bins, ranging from 3 to 9 (2 to 9) jets for the 3- and 4-jet (soft-lepton) analysis. These inputs are shown in the bottom half of Figures 1 and 2.

2. Transfer factors (TF), derived from simulation, relate the W+jets and $t\bar{t}$ normalizations obtained in the control regions to the signal regions. TF's also account for the cross-contamination of different background types between control regions. The contamination of the control regions due to signal events is also treated when testing a specific SUSY model.

3. The number of multijet background events in all control and signal regions, as derived from the data.

4. Expectations from simulation for the number of events from the minor backgrounds (single-top, diboson) in all control and signal regions.

The event count from each of these sources in each of these 14 bins (7 jet multiplicity bins for each of W+jets and $t\bar{t}$; 16 bins in the soft-lepton analysis) is treated with a Poisson probability density function. From this point onward, the electron and muon channels are combined. The statistical and systematic uncertainties on the expected values are included in the probability density function as nuisance parameters, typically constrained to be Gaussian with a width given by the size of the uncertainty. Correlations in the nuisance parameters from bin to bin are taken into account where necessary. The probability density functions also include free parameters, for example to scale the expected contributions from the major backgrounds; these are described in more detail below. A likelihood is formed as the product of these probability density functions and the constraints on the nuisance parameters. The free parameters and nuisance parameters are adjusted to maximize the likelihood. An important difference with respect to the analysis in Ref. [16] is the increase in the number of measurements, allowing the fit to be over-constrained. This has been used in this analysis to constrain the nuisance parameters for b-tagging in the control regions and the uncertainty in the ALPGEN matching scale parameter $k_{T_{fac}}$ from the shape information provided in the control regions. The uncertainty on the JES is not further constrained by the likelihood fit.

The free parameters considered in the fit are as follows:

1. $t\bar{t}$ background: All $t\bar{t}$ samples are scaled by one free parameter for the overall normalization.

2. W/Z background: All W+jets and Z+jets samples are scaled by a common free parameter for the overall normalization.

The backgrounds from multijets and the lesser backgrounds from single-top and diboson production are allowed to float in the fit within their respective uncertainties.

Notable nuisance parameters in the fit are:

1. The uncertainty in the ALPGEN matching scale parameter $k_{T_{fac}}$ manifests itself as a shift in the relative normalization of the different ALPGEN N_{parton} samples. These shifts are mapped to one nuisance parameter. One common nuisance parameter is used for both W+jets and Z+jets processes. A separate parameter is used for $t\bar{t}$.

2. The uncertainty in the ALPGEN MLM-matching parameter $p_{\mathrm{T,min}}$ also manifests itself in the relative normalization of the ALPGEN N_{parton} samples. This shift in the relative normalization is parametrized by one parameter for both W+jets and Z+jets and a separate parameter for $t\bar{t}$.

The background fit is cross-checked in a number of validation regions, situated between the control- and signal regions, where the results of the background fit can be compared to observation. These validation regions are not used to constrain the fit. For the 3- and 4-jet analyses, one common set of validation regions, which receives contributions from both channels, is defined as follows:

1. The W+jets validation region is identical to the W+jets control region for the 3-jet channel except that the $E_{\mathrm{T}}^{\mathrm{miss}}$ requirement is changed to 120 GeV < $E_{\mathrm{T}}^{\mathrm{miss}}$< 250 GeV.

2. Similarly, the $t\bar{t}$ validation region is identical to the $t\bar{t}$ control region for the 3-jet channel except for the change in the $E_{\mathrm{T}}^{\mathrm{miss}}$ requirement to 120 GeV < $E_{\mathrm{T}}^{\mathrm{miss}}$< 250 GeV.

3. The high transverse mass validation region is defined by m_{T} > 80 GeV and 30 GeV < $E_{\mathrm{T}}^{\mathrm{miss}}$< 250 GeV. This region tests the validity of the background from dileptonic $t\bar{t}$.

For the soft-lepton analysis, the validation region is equivalent to the combination of the W+jets and $t\bar{t}$ control regions but with the transverse mass selection changed to 80 GeV < M_{T} < 100 GeV. The results of the fit to the control regions are shown in Table 4 for the 3- and 4-jet channels and in Table 5 for the soft-lepton analysis. Good agreement is seen between predicted and observed values in all regions. The background uncertainties are dominated by systematic uncertainties in the 3-jet channel; in the 4-jet channel, statistical and systematic uncertainties contribute approximately equally. The dominant source of systematic uncertainty for both channels is the jet energy scale, followed by statistics of simulated background samples. The main uncertainties in the soft-lepton analysis come roughly equally from the jet energy scale and the modeling of the W+jets background. The background uncertainties arising from the ALPGEN parameter $k_{T_{fac}}$ are reduced by about a factor of two due to the fit to the jet multiplicity distributions in the control regions.

10 Results and Interpretation

The fit in the signal region proceeds in the same way except that the number of events observed in the signal region is added as an input to the fit and an additional parameter for the non-SM signal strength, constrained to be non-negative, is fit. The results of this fit are shown in Table 6. The number of events observed is found to be consistent with SM expectations in all signal regions. The final $m_{\mathrm{eff}}^{\mathrm{inc}}$ distributions for the 3- and 4-jet channels and the $E_{\mathrm{T}}^{\mathrm{miss}}/m_{\mathrm{eff}}$ distribution for the soft lepton analysis, after the application of all other selection criteria, are shown in Figure 3.

Model-independent limits on the visible cross section (i.e. the cross section evaluated inside the signal region) are derived from the signal fits. Limits on the number of non-SM events in the signal region, derived using the CL_s [60] prescription, are divided by the integrated luminosity to obtain the limits on the visible cross section. The limits at 95% confidence level (CL) are shown in Table 7.

For excluding specific models of new physics, the likelihood fit makes use of the $m_{\mathrm{eff}}^{\mathrm{inc}}$ shape information in the signal region as a further discriminant; these $m_{\mathrm{eff}}^{\mathrm{inc}}$ distributions are shown for the 3- and 4-jet channels in the top half of Figure 3. The likelihood is extended to include bin-by-bin $m_{\mathrm{eff}}^{\mathrm{inc}}$ information by dividing the signal region into six bins of equal width for $m_{\mathrm{eff}}^{\mathrm{inc}}$ between 400 and 1600 GeV, where the last bin is integrated over higher values of $m_{\mathrm{eff}}^{\mathrm{inc}}$. In addition, the expected contamination of control regions due to signal, taken from simulation, is taken into account in the fit. The 3- and 4-jet channels are used to set limits in the MSUGRA/CMSSM model with the same parameters as in Ref. [16]: $\tan\beta = 10$, $A_0 = 0$ and $\mu > 0$, and scanning through the mass parameters m_0 and $m_{1/2}$. The 3- and 4-jet channels

3- and 4-jet channels	W+jets validation	$t\bar{t}$ validation	High m_T validation	$t\bar{t}$ control	W+jets control
Observed events	5281	2458	36041	11143	21324
Fitted bkg events	5300 ± 1000	2600 ± 400	37000 ± 5000	11140 ± 140	21320 ± 150
Fitted top events	1200 ± 220	2180 ± 350	15000 ± 2200	8900 ± 500	4100 ± 500
Fitted W/Z+jets events	3800 ± 900	230 ± 50	18800 ± 2900	1150 ± 120	15000 ± 1100
Fitted other bkg events	181 ± 27	186 ± 22	1170 ± 100	580 ± 60	450 ± 50
Fitted multijet events	9 ± 80	7 ± 50	1300 ± 1600	500 ± 400	1800 ± 1300
MC exp. SM events	5700	2600	39000	11220	22900
MC exp. top events	1290	2220	15500	9000	4300
MC exp. W/Z+jets events	4200	250	20700	1240	16400
MC exp. other bkg events	181	183	1170	560	440
Data-driven multijet events	9	7	1300	400	1700

Table 4: Results of the background fit to the control regions for the 3- and 4-jet analyses. The prediction in the validation region is also shown. The sum of the fitted background estimates listed by process may not add up to the total fitted background because of numerical rounding. The inputs to the fit are also shown; these consist of the data-driven multijet background estimate and the nominal expectations from simulation (MC), normalized to theoretical cross-sections. The errors shown are the statistical plus systematic uncertainties; there is a strong negative correlation between the uncertainties for the fitted $t\bar{t}$ versus W/Z+jets events.

Soft lepton channel	Validation Region	$t\bar{t}$ Control	W+jets Control
Observed events	764	271	1794
Fitted bkg events	810 ± 230	268 ± 17	1800 ± 50
Fitted top events	160 ± 40	169 ± 24	143 ± 32
Fitted W/Z+jets events	600 ± 200	55 ± 10	1550 ± 60
Fitted other bkg events	30 ± 8	30 ± 4	40 ± 5
Fitted multijet events	30 ± 40	14 ± 16	60 ± 70
MC exp. SM events	820	237	1810
MC exp. top events	160	157	164
MC exp. W/Z+jets events	600	43	1540
MC exp. other bkg events	29	25	41
Data-driven multijet events	31	12	60

Table 5: Results of the background fit to the control regions for the soft-lepton channel. The prediction in the validation region is also shown. The sum of the fitted background estimates listed by process may not add up to the total fitted background because of numerical rounding. The inputs to the fit are also shown; these consist of the data-driven multijet background estimate and the nominal expectations from simulation (MC), normalized to theoretical cross-sections. The errors shown are the statistical plus systematic uncertainties; there is a strong negative correlation between the uncertainties for the fitted $t\bar{t}$ versus W/Z+jets events.

	3-jet	4-jet	soft lepton
Observed events	3	6	26
Fitted bkg events	5.7 ± 4.0	8.3 ± 3.1	32 ± 11
Fitted top events	2.0 ± 1.5	5.3 ± 2.1	8.6 ± 3.4
Fitted W/Z+jets events	2.9 ± 2.1	2.0 ± 0.7	15 ± 7
Fitted other bkg events	0.5 ± 0.7	0.9 ± 0.8	0.62 ± 0.24
Fitted multijet events	0.3 ± 0.4	0.17 ± 0.30	8 ± 4
MC exp. SM events	5.6	7.9	32
MC exp. top events	1.9	5.0	8.6
MC exp. W/Z+jets events	3.1	2.0	15
MC exp. other bkg events	0.3	0.7	0.62
Data-driven multijet events	0.3	0.17	8

Table 6: Results of the fit in the signal regions. The inputs to the fit are also shown; these consist of the data-driven multijet background estimate and the nominal expectations from simulation (MC), normalized to theoretical cross-sections. The errors shown are the statistical plus systematic uncertainties; there is a strong negative correlation between the uncertainties for the fitted $t\bar{t}$ versus W/Z+jets events.

Signal channel	$\langle\epsilon\sigma\rangle^{95}_{\rm obs}$[fb]	$S^{95}_{\rm obs}$	$S^{95}_{\rm exp}$	CL_B
3-jet	1.3	6.1	$7.2^{+3.0}_{-2.1}$	0.31
4-jet	1.5	7.2	$8.0^{+3.5}_{-2.4}$	0.36
soft-lepton	3.7	17.2	20^{+7}_{-5}	0.32

Table 7: 95% CL upper limits on the visible cross-section ($\langle\epsilon\sigma\rangle^{95}_{\rm obs}$) and on the observed ($S^{95}_{\rm obs}$) and expected ($S^{95}_{\rm exp}$) number of signal events. The last column indicates the CL_B value, i.e. the confidence level observed for the background-only hypothesis. All numbers are given for the combination of electron and muon channels.

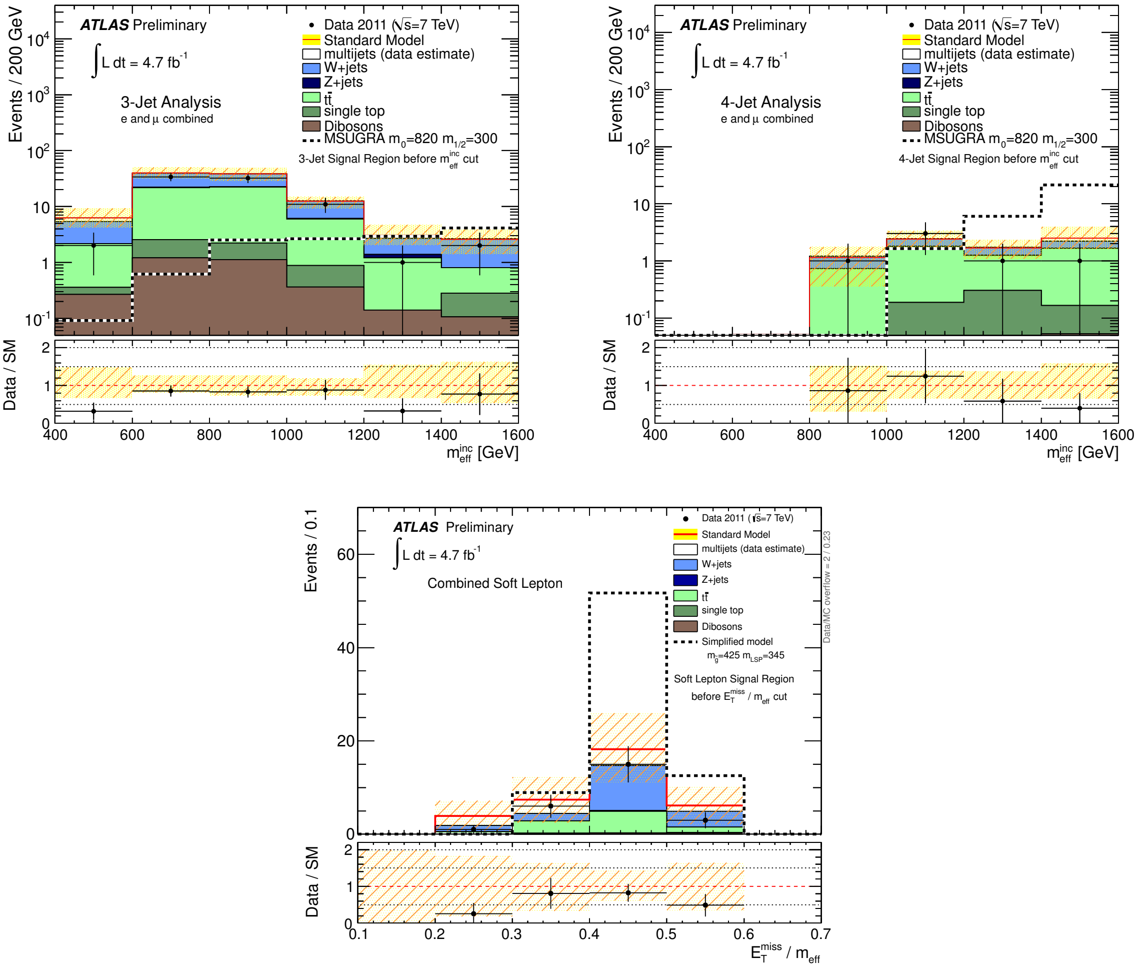

Figure 3: Distributions of $m_{\mathrm{eff}}^{\mathrm{inc}}$ in the 3-jet (top left) and 4-jet (top right) signal regions after all cuts have been applied except for the cut on the inclusive effective mass. The last $m_{\mathrm{eff}}^{\mathrm{inc}}$ bin is inclusive, and includes all overflows. The lowest $m_{\mathrm{eff}}^{\mathrm{inc}}$ bins are affected by the minimum p_{T} requirements on jets and $E_{\mathrm{T}}^{\mathrm{miss}}$. The plot on the bottom shows the $E_{\mathrm{T}}^{\mathrm{miss}}/m_{\mathrm{eff}}$ distribution in the soft-lepton signal region after all cuts except for the $E_{\mathrm{T}}^{\mathrm{miss}}/m_{\mathrm{eff}}$ cut. Electron and muon channels have been combined. The "Data/SM" plots show the ratio between data and the summed Standard Model expectation. The Standard Model expectation shown here is derived from simulation only, normalized to the theoretical cross sections. The uncertainty band on the Standard Model expectation shown here combines the statistical uncertainty on the simulated event samples with the systematic uncertainties on the jet energy scale, b-tagging, data-driven multijet background, and luminosity. The systematic uncertainties are largely correlated from bin to bin.

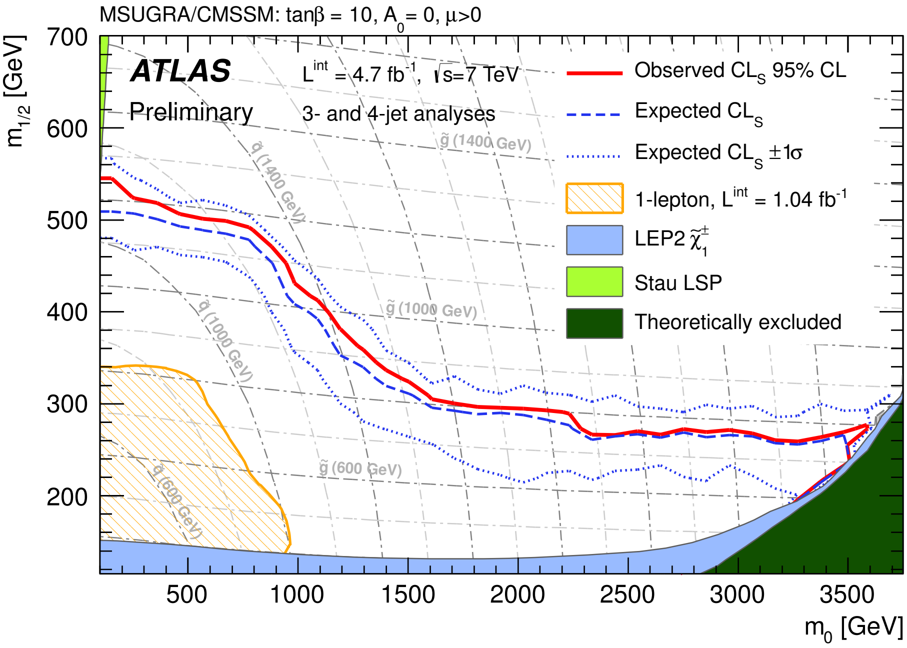

Figure 4: Expected and observed 95% CL exclusion limits, as well as the ±1 sigma variation on the median expected limit, combining the electron and muon channels in the 3- and 4-jet analyses. The previous limit from ATLAS and the results from the LEP experiments are also shown. The dashed grey lines show contours of constant squark (curved lines) and gluino (nearly horizontal lines) masses.

are statistically independent, and the exclusion limits from these two channels are combined for the final result. The soft-lepton channel is used in addition to set limits in a one-step simplified model with $\tilde{g}\tilde{g}$ pair production followed by the decay $\tilde{g} \to q\bar{q}'\tilde{\chi}_1^{\pm} \to q\bar{q}'W^{\pm}\tilde{\chi}_1^0$ where the W can be virtual and decays according to SM branching ratios. The chargino mass is fixed in this case to be halfway in between the gluino and $\tilde{\chi}_1^0$ masses.

Systematic uncertainties on the SUSY signal acceptance arising from detector effects are treated in the same way as for the background simulated samples. Uncertainties on the signal cross section are treated as follows. An envelope of cross section predictions is defined using the 68% C.L. ranges of the CTEQ6 [61] (including the α_S uncertainty) and MSTW [62] PDF sets, together with independent variations of the factorization and renormalization scales by factors of two or one half. The nominal cross section value is taken to be the midpoint of the envelope and the uncertainty assigned is half the full width of the envelope, closely following the PDF4LHC recommendations [63]. Uncertainties are calculated for individual SUSY production processes. The dominant uncertainties in the region of the MSUGRA/CMSSM model where the exclusion limits are placed arise from the PDF's (30-40%) and the JES (10-20%); the former reflect the uncertainty in the high-x gluon density. For the simplified models, uncertainties in the modeling of initial-state radiation play a significant role for low gluino masses and for small mass differences in the decay cascade. These uncertainties are estimated by varying generator parameters in the simulation as well as by generator-level studies of $\tilde{g}\tilde{g}$ and production with an additional ISR jet generated in the matrix element with MADGRAPH5 [26]. Typical uncertainties for small mass differences are approximately 30%.

The limit in the plane of $m_{1/2}$ versus m_0 in the MSUGRA/CMSSM model is shown in Figure 4. A large improvement in exclusion reach over the previous analysis [16] can be seen. The simultaneous fit to the 3- and 4-jet signal regions and the inclusion into the fit of the shapes of the $m_{\rm eff}^{\rm inc}$ distributions within those signal regions increases the mass reach by about 100 GeV in the $m_{1/2}$ versus m_0 plane. Along the line of equal masses between squarks and gluinos in the MSUGRA/CMSSM model, masses below approximately 1200 GeV are excluded at 95% CL.

For the simplified model, exclusion limits are set in the plane of the $\tilde{\chi}_1^0$ mass versus the gluino mass, as shown in Figure 5 (left) for the 3- and 4-jet analyses combined and Figure 5 (right) for the soft-lepton analysis. In Fig. 5 (right) the observed limit can be better or worse than the expected limit depending on the signal grid point, the bins in which they appear in the $E_{\mathrm{T}}^{\mathrm{miss}}/m_{\mathrm{eff}}$ distribution, and the amount of signal contamination in the background control regions. For LSP masses below 200 GeV, gluinos in this model are excluded for masses below approximately 900 GeV. The figures also show the cross section for this model excluded at 95% CL. In the region near the diagonal where the gluino and $\tilde{\chi}_1^0$ masses are almost degenerate, the cross section excluded by the soft-lepton analysis is 20-30 times smaller than the combination of the 3- and 4-jet analyses.

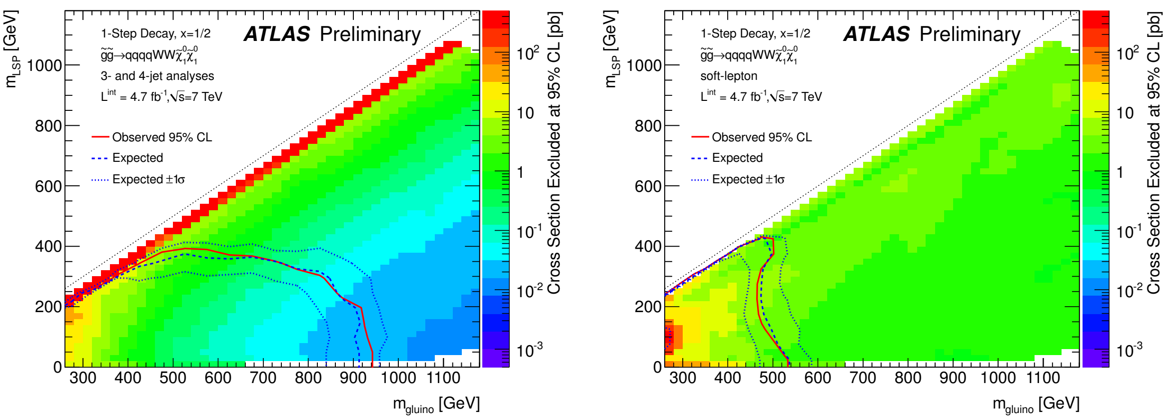

Figure 5: Excluded cross sections at 95% confidence level for a simplified model with gluino pair production, followed by the decay $\tilde{g} \rightarrow q\bar{q}'\tilde{\chi}_1^{\pm} \rightarrow q\bar{q}'W^{\pm}\tilde{\chi}_1^0$ where the W decays according to SM branching ratios. The chargino mass is taken to be halfway in between the gluino and $\tilde{\chi}_1^0$ masses. The plot on the left is from the combination of the 3- and 4-jet channels, while the plot on the right is from the soft-lepton analysis. The color code shows the excluded cross section in pb. A smaller excluded cross-section implies a more stringent limit. The ±1 sigma variation on the median expected limit is also shown.

11 Conclusion

In this note an update is presented of the search with the ATLAS detector for SUSY in final states containing jets, one isolated lepton (electron or muon) and $E_{\mathrm{T}}^{\mathrm{miss}}$. Compared to the previous analysis in this channel by ATLAS [16], the integrated luminosity is increased from approximately 1 fb^{-1} to about 4.7 fb^{-1}. A new signal region with a soft lepton and soft jets has been introduced to be sensitive to SUSY decay spectra involving small mass differrences. For the first time in ATLAS SUSY searches, a simultaneous fit is performed to multiple signal regions and to the shapes of distributions within those signal regions. This increases the mass reach for this analysis by about 100 GeV. The inclusion into the fit of the shapes of multiple background distributions has been used to reduce the background uncertainties arising from the ALPGEN parameter $k_{T_{fac}}$ by about a factor of two.

Observations are in good agreement with SM expectations and limits have been extended on the visible cross section for new physics processes. Exclusion limits have also been extended for the MSUGRA/CMSSM model and one-step simplified models. In the MSUGRA/CMSSM model, squark and gluino masses below approximately 1200 GeV are excluded at 95% CL (for equal squark and gluino masses). In the one-step simplified model considered here, gluinos with mass below aproximately 900 GeV are excluded at 95% CL if the LSP has a mass below 200 GeV. In addition, the exclusion limits in this model have been extended significantly in the low mass-difference region; the new signal region defined by soft leptons and jets improves the excluded cross section in the low mass-difference region by a factor of 20-30 compared to the 3- and 4-jet analyses.

References

[1] H. Miyazawa, *Baryon Number Changing Currents*, Prog. Theor. Phys. **36 (6)** (1966) 1266–1276.

[2] P. Ramond, *Dual Theory for Free Fermions*, Phys. Rev. **D3** (1971) 2415–2418.

[3] Y. A. Golfand and E. P. Likhtman, *Extension of the Algebra of Poincare Group Generators and Violation of p Invariance*, JETP Lett. **13** (1971) 323–326. [Pisma Zh. Eksp. Teor. Fiz. 13:452-455,1971].

[4] A. Neveu and J. H. Schwarz, *Factorizable dual model of pions*, Nucl. Phys. **B31** (1971) 86–112.

[5] A. Neveu and J. H. Schwarz, *Quark Model of Dual Pions*, Phys. Rev. **D4** (1971) 1109–1111.

[6] J. Gervais and B. Sakita, *Field theory interpretation of supergauges in dual models*, Nucl. Phys. **B34** (1971) 632–639.

[7] D. V. Volkov and V. P. Akulov, *Is the Neutrino a Goldstone Particle?*, Phys. Lett. **B46** (1973) 109–110.

[8] J. Wess and B. Zumino, *A Lagrangian Model Invariant Under Supergauge Transformations*, Phys. Lett. **B49** (1974) 52.

[9] J. Wess and B. Zumino, *Supergauge Transformations in Four-Dimensions*, Nucl. Phys. **B70** (1974) 39–50.

[10] L. Evans and P. Bryant (editors), *LHC Machine*, JINST **3** (2008) S08001.

[11] P. Fayet, *Supersymmetry and Weak, Electromagnetic and Strong Interactions*, Phys. Lett. **B64** (1976) 159.

[12] P. Fayet, *Spontaneously Broken Supersymmetric Theories of Weak, Electromagnetic and Strong Interactions*, Phys. Lett. **B69** (1977) 489.

[13] G. R. Farrar and P. Fayet, *Phenomenology of the Production, Decay, and Detection of New Hadronic States Associated with Supersymmetry*, Phys. Lett. **B76** (1978) 575–579.

[14] P. Fayet, *Relations Between the Masses of the Superpartners of Leptons and Quarks, the Goldstino Couplings and the Neutral Currents*, Phys. Lett. **B84** (1979) 416.

[15] S. Dimopoulos and H. Georgi, *Softly Broken Supersymmetry and SU(5)*, Nucl. Phys. **B193** (1981) 150.

[16] ATLAS Collaboration, *Search for supersymmetry in final states with jets, missing transverse momentum and one isolated lepton in $\sqrt{s} = 7$ TeV collisions using 1 fb^{-1} of ATLAS data*, Phys. Rev. **D85** (2012) 012006.

[17] CMS Collaboration, *Search for new physics with single leptons at the LHC*, CMS-PAS-SUS-11-015 (2011) . (https://cdsweb.cern.ch/record/1380922).

[18] ATLAS Collaboration, *The ATLAS Experiment at the CERN Large Hadron Collider*, JINST **3** (2008) S08003.

[19] ATLAS Collaboration, *Expected Performance of the ATLAS Experiment - Detector, Trigger and Physics*, `arXiv:0901.0512 [hep-ex]`.

[20] A.H. Chamseddine, R.L. Arnowitt and P. Nath, Phys. Rev. Lett. **49** (1982) 970; R. Barbieri, S. Ferrara and C.A. Savoy, Phys. Lett. **B119** (1982) 343; L.E. Ibanez, Phys. Lett. **B118** (1982) 73; L.J. Hall, J.D. Lykken and S. Weinberg, Phys. Rev. **D27** (1983) 2359; N. Ohta, Prog. Theor. Phys. **70** (1983) 542.

[21] G. L. Kane, C. F. Kolda, L. Roszkowski, and J. D. Wells, *Study of constrained minimal supersymmetry*, Phys. Rev. **D49** (1994) 6173–6210, `arXiv:hep-ph/9312272 [hep-ph]`.

[22] J. Alwall, P. Schuster, and N. Toro, *Simplified Models for a First Characterization of New Physics at the LHC*, Phys. Rev. **D79** (2009) 075020, `arXiv:0810.3921 [hep-ph]`.

[23] LHC New Physics Working Group Collaboration, D. Alves et al., *Simplified Models for LHC New Physics Searches*, `arXiv:1105.2838 [hep-ph]`.

[24] M. Bahr, S. Gieseke, M. Gigg, D. Grellscheid, K. Hamilton, et al., *Herwig++ Physics and Manual*, Eur. Phys. J. **C58** (2008) 639–707, `arXiv:0803.0883 [hep-ph]`.

[25] F. E. Paige, S. D. Protopopescu, H. Baer, and X. Tata, *ISAJET 7.69: A Monte Carlo event generator for pp, anti-p p, and e+e- reactions*, `arXiv:hep-ph/0312045 [hep-ph]`.

[26] J. Alwall, M. Herquet, F. Maltoni, O. Mattelaer, and T. Stelzer, *MadGraph 5 : Going Beyond*, JHEP **1106** (2011) 128, `arXiv:1106.0522 [hep-ph]`.

[27] J. Pumplin, D. Stump, J. Huston, H. Lai, P. M. Nadolsky, et al., *New generation of parton distributions with uncertainties from global QCD analysis*, JHEP **0207** (2002) 012, `arXiv:hep-ph/0201195 [hep-ph]`.

[28] J. Alwall, S. Hoche, F. Krauss, N. Lavesson, L. Lonnblad, et al., *Comparative study of various algorithms for the merging of parton showers and matrix elements in hadronic collisions*, Eur. Phys. J. **C53** (2008) 473–500, `arXiv:0706.2569 [hep-ph]`.

[29] W. Beenakker, R. Hopker, M. Spira, and P. Zerwas, *Squark and gluino production at hadron colliders*, Nucl. Phys. **B492** (1997) 51–103, `arXiv:hep-ph/9610490 [hep-ph]`.

[30] A. Kulesza and L. Motyka, *Threshold resummation for squark-antisquark and gluino-pair production at the LHC*, Phys. Rev. Lett. **102** (2009) 111802, `arXiv:0807.2405 [hep-ph]`.

[31] A. Kulesza and L. Motyka, *Soft gluon resummation for the production of gluino-gluino and squark-antisquark pairs at the LHC*, Phys. Rev. **D80** (2009) 095004, `arXiv:0905.4749 [hep-ph]`.

[32] W. Beenakker, S. Brensing, M. Kramer, A. Kulesza, E. Laenen, et al., *Soft-gluon resummation for squark and gluino hadroproduction*, JHEP **0912** (2009) 041, `arXiv:0909.4418 [hep-ph]`.

[33] W. Beenakker, S. Brensing, M. Kramer, A. Kulesza, E. Laenen, et al., *Squark and gluino hadroproduction*, Int. J. Mod. Phys. **A26** (2011) 2637–2664, `arXiv:1105.1110 [hep-ph]`.

[34] M. L. Mangano, M. Moretti, F. Piccinini, R. Pittau, and A. D. Polosa, *ALPGEN, a generator for hard multiparton processes in hadronic collisions*, JHEP **0307** (2003) 001, arXiv:hep-ph/0206293 [hep-ph].

[35] M. Aliev, H. Lacker, U. Langenfeld, S. Moch, P. Uwer, et al., *HATHOR: HAdronic Top and Heavy quarks crOss section calculatoR*, Comput. Phys. Commun. **182** (2011) 1034–1046, arXiv:1007.1327 [hep-ph].

[36] K. Melnikov and F. Petriello, *Electroweak gauge boson production at hadron colliders through O(alpha(s)**2)*, Phys. Rev. **D74** (2006) 114017, arXiv:hep-ph/0609070 [hep-ph].

[37] S. Frixione and B. R. Webber, *Matching NLO QCD computations and parton shower simulations*, JHEP **0206** (2002) 029, arXiv:hep-ph/0204244 [hep-ph].

[38] G. Corcella, I. Knowles, G. Marchesini, S. Moretti, K. Odagiri, et al., *HERWIG 6: An Event generator for hadron emission reactions with interfering gluons (including supersymmetric processes)*, JHEP **0101** (2001) 010, arXiv:hep-ph/0011363 [hep-ph].

[39] J. M. Campbell, R. Ellis, and D. L. Rainwater, *Next-to-leading order QCD predictions for W + 2 jet and Z + 2 jet production at the CERN LHC*, Phys. Rev. **D68** (2003) 094021, arXiv:hep-ph/0308195 [hep-ph].

[40] J. Butterworth, J. R. Forshaw, and M. Seymour, *Multiparton interactions in photoproduction at HERA*, Z. Phys. **C72** (1996) 637–646, arXiv:hep-ph/9601371 [hep-ph].

[41] H.-L. Lai, M. Guzzi, J. Huston, Z. Li, P. M. Nadolsky, et al., *New parton distributions for collider physics*, Phys. Rev. **D82** (2010) 074024, arXiv:1007.2241 [hep-ph].

[42] A. Sherstnev and R. Thorne, *Different PDF approximations useful for LO Monte Carlo generators*, arXiv:0807.2132 [hep-ph].

[43] ATLAS Collaboration, *New ATLAS event generator tunes to 2010 data*, ATL-PHYS-PUB-2011-008 (2011) . (https://cdsweb.cern.ch/record/1345343).

[44] A. Martin, W. Stirling, R. Thorne, and G. Watt, *Update of parton distributions at NNLO*, Phys. Lett. **B652** (2007) 292–299, arXiv:0706.0459 [hep-ph].

[45] ATLAS Collaboration, *The ATLAS Simulation Infrastructure*, Eur. Phys. J. **C70** (2010) 823–874, arXiv:1005.4568 [physics.ins-det].

[46] GEANT4 Collaboration, S. Agostinelli et al., *GEANT4: A Simulation toolkit*, Nucl. Instrum. Meth. **A506** (2003) 250–303.

[47] T. Gleisberg, S. Hoeche, F. Krauss, M. Schonherr, S. Schumann, et al., *Event generation with SHERPA 1.1*, JHEP **0902** (2009) 007, arXiv:0811.4622 [hep-ph].

[48] ATLAS Collaboration, *Electron performance measurements with the ATLAS detector using the 2010 LHC proton-proton collision data*, arXiv:1110.3174 [hep-ex].

[49] ATLAS Collaboration, *A measurement of the ATLAS muon reconstruction and trigger efficiency using J/psi decays*, ATLAS-CONF-2011-021 (2011) . (https://cdsweb.cern.ch/record/1336750.

[50] ATLAS Collaboration, *Muon reconstruction efficiency in reprocessed 2010 LHC proton-proton collision data recorded with the ATLAS detector*, ATLAS-CONF-2011-063 (2011) . (https://cdsweb.cern.ch/record/1345743).

[51] M. Cacciari, G. P. Salam, and G. Soyez, *The anti-k_t jet clustering algorithm*, JHEP **04** (2008) 063, arXiv:0802.1189 [hep-ph].

[52] M. Cacciari and G. P. Salam, *Dispelling the N^3 myth for the k_t jet-finder*, Phys. Lett. **B641** (2006) 57–61, arXiv:hep-ph/0512210.

[53] ATLAS Collaboration, *Jet energy measurement with the ATLAS detector in proton-proton collisions at $\sqrt{s}$ = 7 TeV*, arXiv:1112.6426 [hep-ex]. Submitted to *Eur. Phys. J. C*.

[54] ATLAS Collaboration, *Performance of primary vertex reconstruction in proton-proton collisions at $\sqrt{s}$ = 7 TeV in the ATLAS experiment*, ATLAS-CONF-2010-069 (2010) . (http://cdsweb.cern.ch/record/1281344).

[55] ATLAS Collaboration, *Commissioning of the ATLAS high-performance b-tagging algorithms in the 7 TeV collision data*, ATLAS-CONF-2011-102 (2011) . (https://cdsweb.cern.ch/record/1369219.

[56] ATLAS Collaboration, *Luminosity Determination in pp Collisions at sqrt(s)=7 TeV Using the ATLAS Detector at the LHC*, Eur. Phys. J. **C71** (2011) 1630, arXiv:1101.2185 [hep-ex].

[57] ATLAS Collaboration, *Luminosity Determination in pp Collisions at sqrt(s) = 7 TeV using the ATLAS Detector in 2011*, ATLAS-CONF-2011-116 (2011) . (https://cdsweb.cern.ch/record/1376384).

[58] ATLAS Collaboration, *Performance of missing transverse momentum reconstruction in proton-proton collisions at 7 TeV with ATLAS*, arXiv:1108.5602 [hep-ex].

[59] G. Cowan, K. Cranmer, E. Gross, and O. Vitells, *Asymptotic formulae for likelihood-based tests of new physics*, Eur. Phys. J. **C71** (2011) 1554, arXiv:1007.1727 [physics.data-an].

[60] A. L. Read, *Presentation of search results: The CL(s) technique*, J. Phys. G **G28** (2002) 2693–2704.

[61] P. M. Nadolsky, H.-L. Lai, Q.-H. Cao, J. Huston, J. Pumplin, et al., *Implications of CTEQ global analysis for collider observables*, Phys. Rev. **D78** (2008) 013004, arXiv:0802.0007 [hep-ph].

[62] A. Martin, W. Stirling, R. Thorne, and G. Watt, *Parton distributions for the LHC*, Eur. Phys. J. **C63** (2009) 189–285, arXiv:0901.0002 [hep-ph].

[63] M. Botje, J. Butterworth, A. Cooper-Sarkar, A. de Roeck, J. Feltesse, et al., *The PDF4LHC Working Group Interim Recommendations*, arXiv:1101.0538 [hep-ph].

[64] ATLAS Collaboration, *Search for squarks and gluinos using final states with jets and missing transverse momentum with the ATLAS detector in $\sqrt{s}$ = 7 TeV proton-proton collisions*, ATLAS-CONF-2012-033 (2012) . (https://cdsweb.cern.ch/record/1432199).

[65] ATLAS Collaboration, *Hunt for new phenomena using large jet multiplicities and missing transverse momentum at ATLAS, in L=4.7 $fb^{-1}$of $\sqrt{s}$ = 7 TeV proton-proton collisions*, ATLAS-CONF-2012-037 (2012) . (https://cdsweb.cern.ch/record/1432204).

A Additional figures

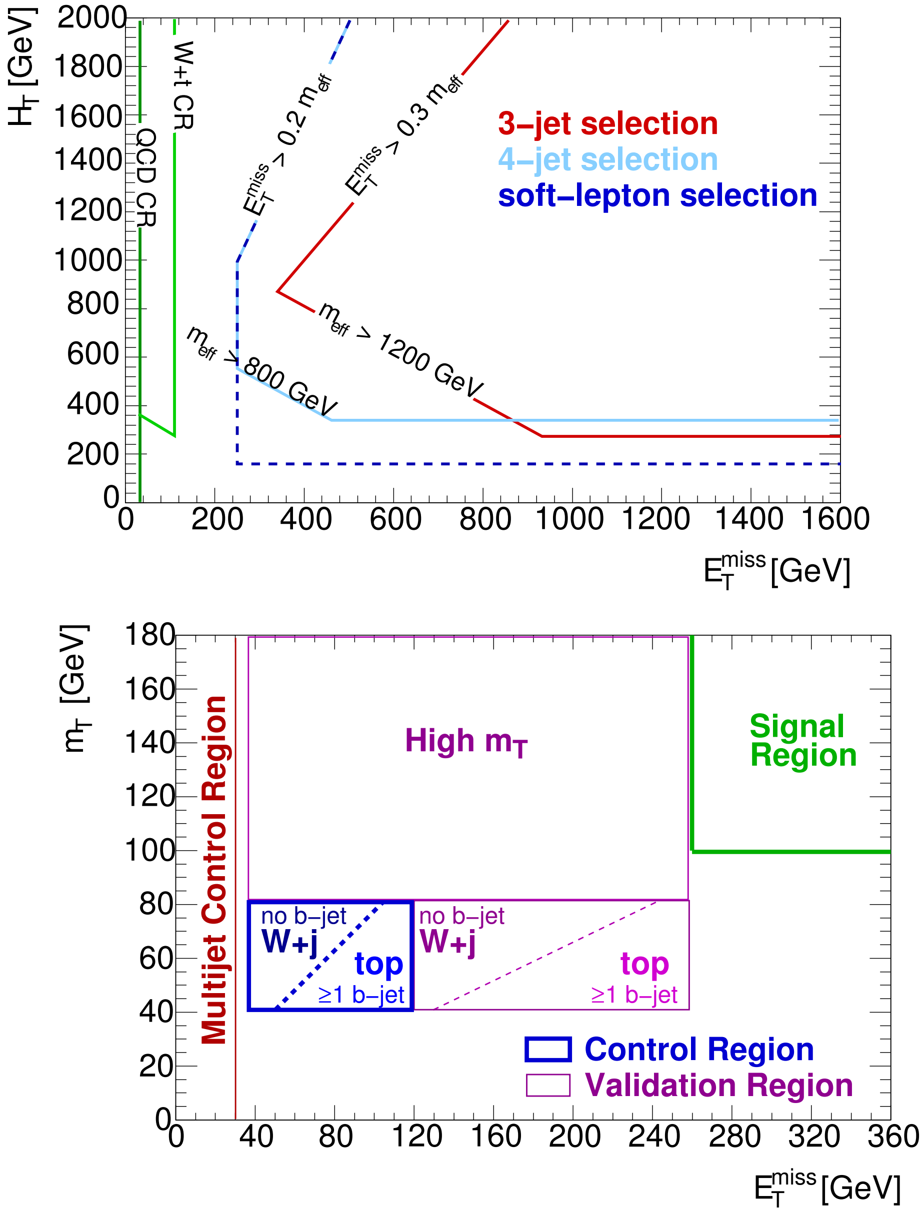

Figure 6: Top: Graphical illustration of the signal regions for this analysis. The regions enriched in W+top and multijet backgrounds are also shown. Bottom: Control and validation regions in the m_T versus E_T^{miss} plane, together with the regions used for the QCD fake estimate.

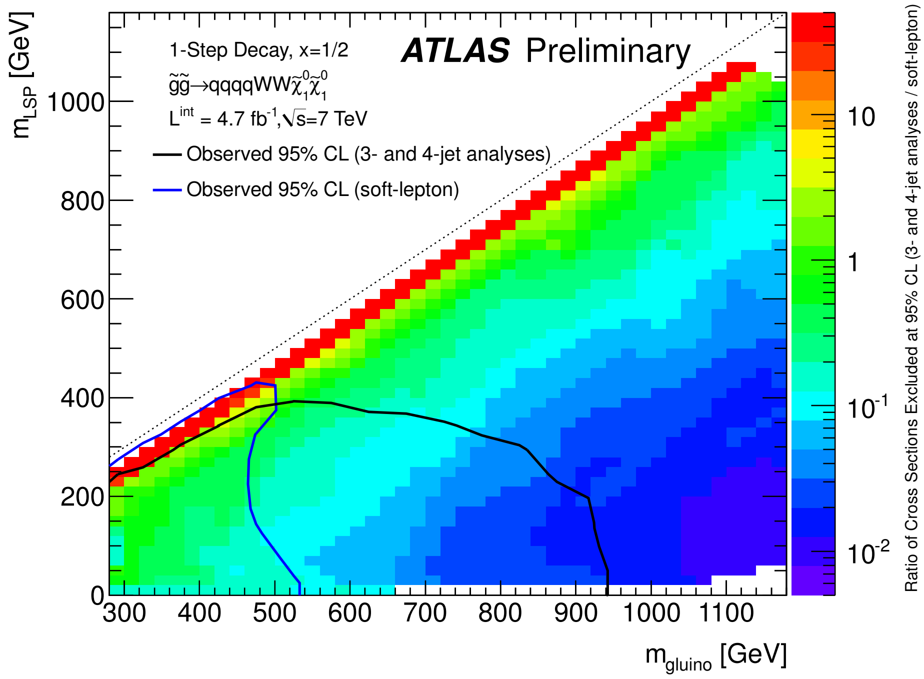

Figure 7: Ratio of the excluded cross sections by the 3- (and 4-jet) analysis (numerator) versus the soft-lepton (denominator), shown on Fig. 5, for a simplified model with gluino production and $x = 1/2$. The soft 1-lepton search is more powerful along the diagonal region where the masses of the gluino and LSP become quasi-degenerate (i.e. *compressed SUSY*) while the 3- and 4-jet analyses are generally more powerful in the rest of the phase space.

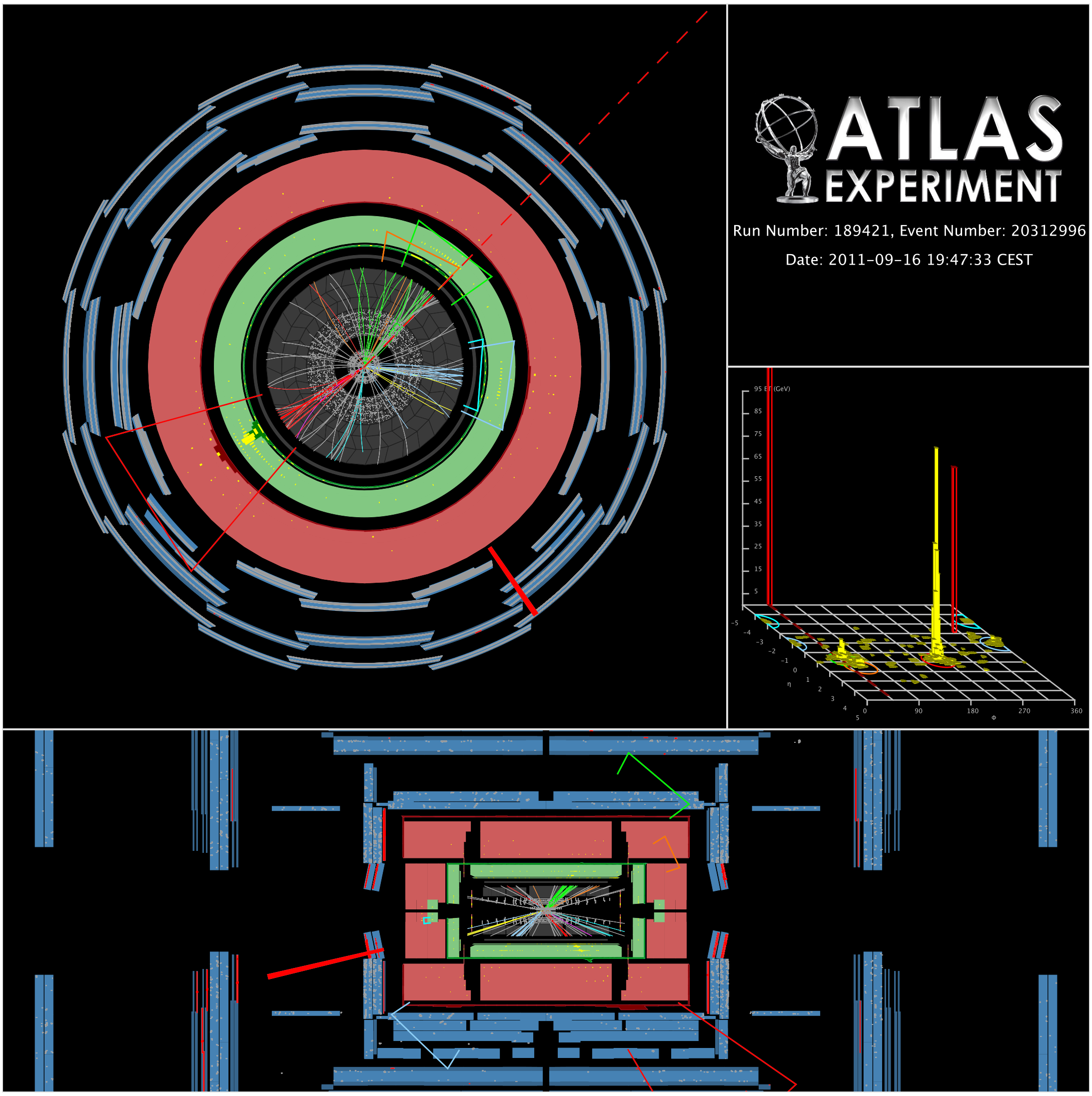

Figure 8: Event display of the muon event with the highest inclusive effective mass, passing the 3-jet selection. The $p_{\rm T}$ of the three leading jets are: 615, 101 and 92 GeV. There is also a fourth jet with $p_{\rm T}$= 58 GeV. The muon $p_{\rm T}$ is 74 GeV and $E_{\rm T}^{\rm miss}$= 409 GeV. The inclusive effective mass is 1350 GeV.

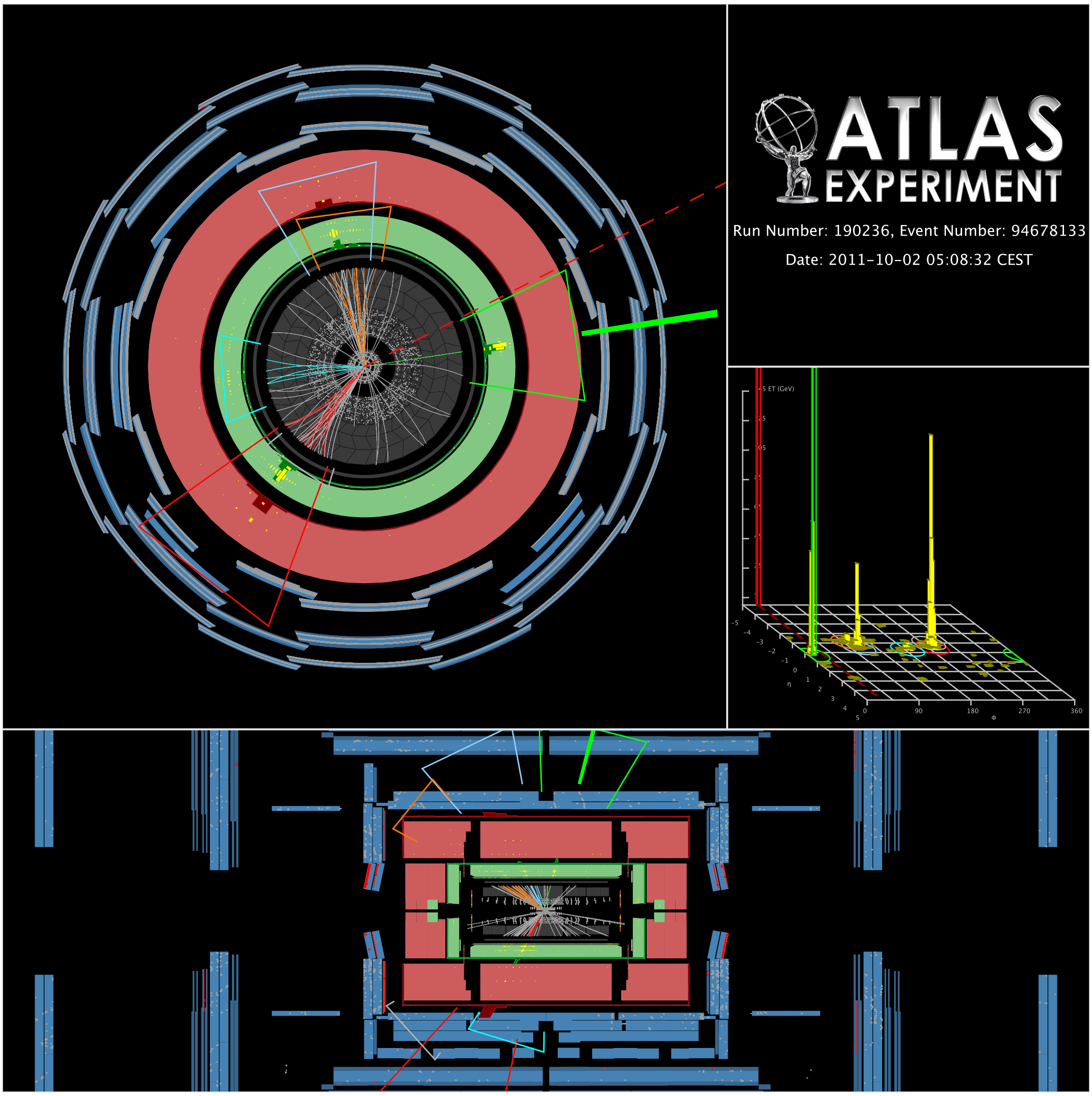

Figure 9: Event display of the electron event with the highest inclusive effective mass, passing the 4-jet selection. The p_{T} of the four leading jets are: 690, 254, 117 and 84 GeV. There is also a fifth jet with p_{T}= 36 GeV. The electron p_{T} is 265 GeV and $E_{\mathrm{T}}^{\mathrm{miss}}$= 381 GeV. The inclusive effective mass is 1827 GeV.

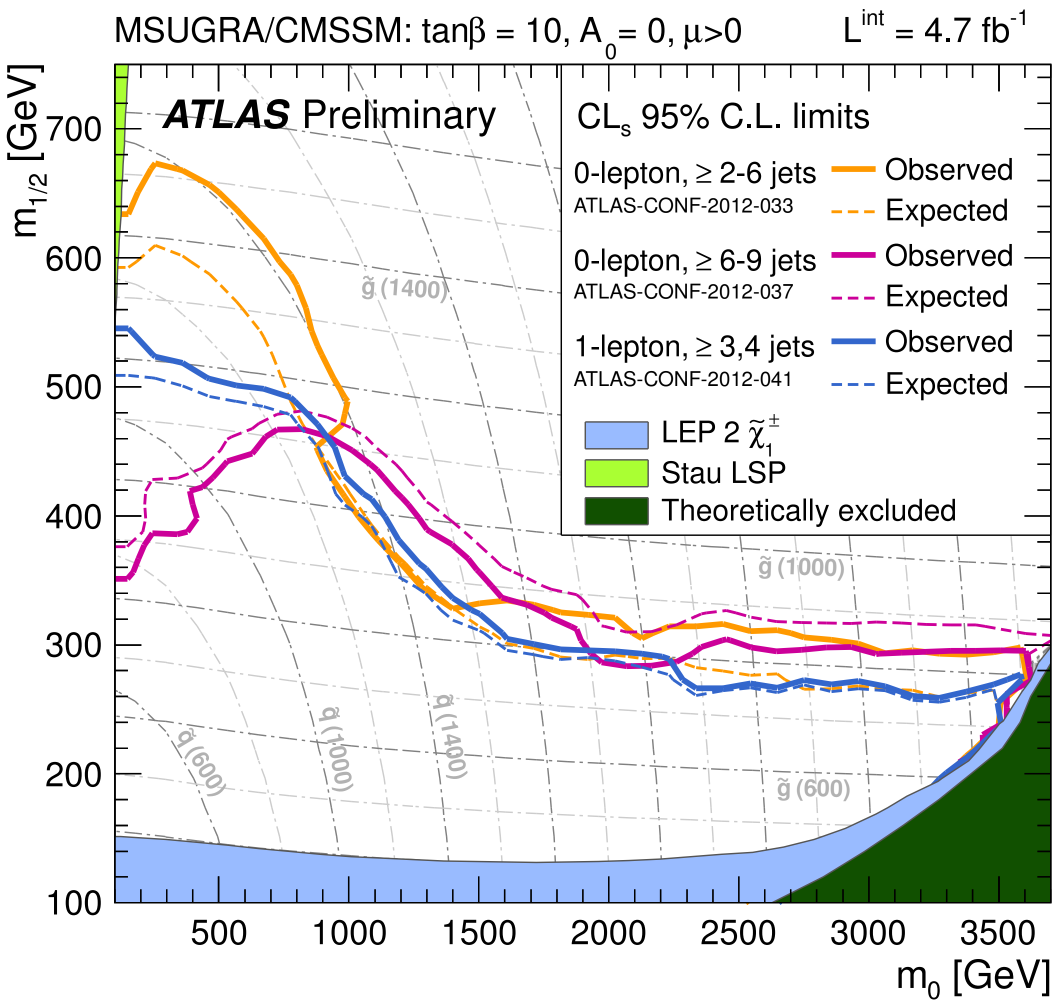

Figure 10: Expected and observed 95% CL exclusion limits in the MSUGRA/CMSSM model, showing the results from three recent ATLAS searches: multijets + $E_{\mathrm{T}}^{\mathrm{miss}}$ [64], high jet multiplicity + $E_{\mathrm{T}}^{\mathrm{miss}}$ [65], and this analysis.

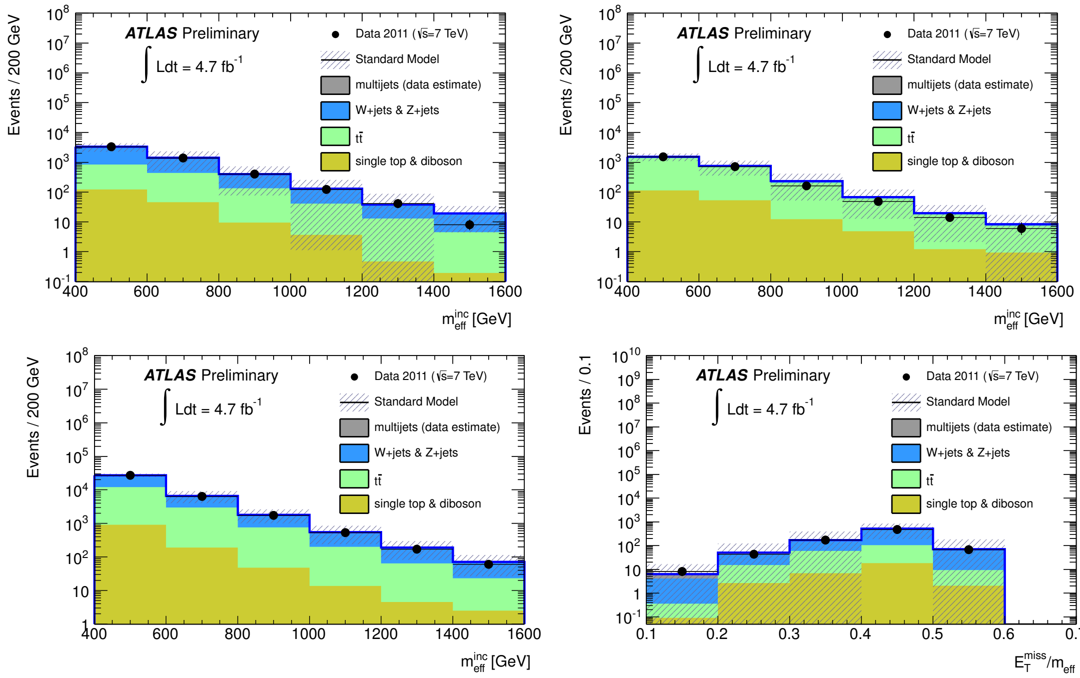

Figure 11: The $m_{\mathrm{eff}}^{\mathrm{inc}}$ distributions in the W (top, left), $t\bar{t}$ (top, right) and high transverse mass (bottom, left) validation regions for the 3- and 4-jet analyses. Bottom right: the $E_{\mathrm{T}}^{\mathrm{miss}}/m_{\mathrm{eff}}$ distribution in the validation region for the soft-lepton analysis.